NANO LETTERS

LETTER

pubs.acs.org/NanoLett

Crystal Structure Transfer in Core/Shell Nanowires

Rienk E. Algra,[†,‡,§,#] Moïra Hocevar,[∥,‡,#] Marcel A. Verheijen,[‡,⊥] Ilaria Zardo,[¶] George G. W. Immink,[‡] Willem J. P. van Enckevort,[§] Gerhard Abstreiter,[¶] Leo P. Kouwenhoven,[∥] Elias Vlieg,[§] and Erik P. A. M. Bakkers*[,∥,⊥]

[†]Materials Innovation Institute (M2i), 2628CD Delft, The Netherlands

[‡]Philips Research Laboratories Eindhoven, High Tech Campus 11, 5656AE Eindhoven, The Netherlands

[§]Institute for Molecules and Materials, Radboud University Nijmegen, Heyendaalseweg 135, 6525AJ Nijmegen, The Netherlands

[∥]Kavli Institute of Nanoscience, Delft University of Technology, 2628 CJ Delft, The Netherlands

[⊥]Photonics and Semiconductor Nanophysics, Department of Applied Physics, Eindhoven University of Technology, 5600 MB Eindhoven, The Netherlands

[¶]Walter Schottky Institut and Physik Department, Technische Universität München, Am Coulombwall 4, 85748 Garching, Germany

Supporting Information

ABSTRACT: Structure engineering is an emerging tool to control opto-electronic properties of semiconductors. Recently, control of crystal structure and the formation of a twinning superlattice have been shown for III−V nanowires. This level of control has not been obtained for Si nanowires, the most relevant material for the semiconductor industry. Here, we present an approach, in which a designed twinning superlattice with the zinc blende crystal structure or the wurtzite crystal structure is transferred from a gallium phosphide core wire to an epitaxially grown silicon shell. These materials have a difference in lattice constants of only 0.4%, which allows for structure transfer without introducing extra defects. The twinning superlattices, periodicity, and shell thickness can be tuned with great precision. Arrays of free-standing Si nanotubes are obtained by a selective wet-chemical etch of the core wire.

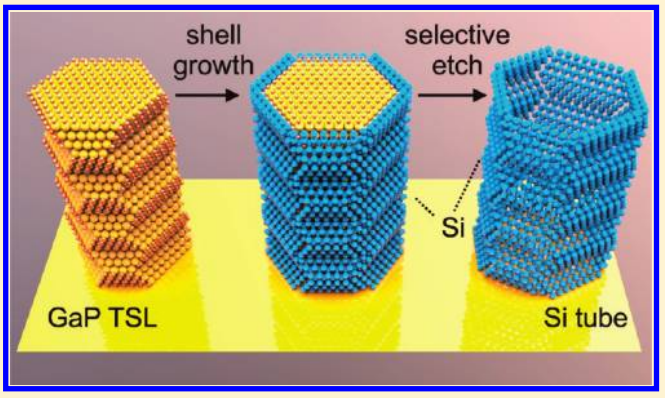

KEYWORDS: Nanowire, structure transfer, epitaxy, superlattice, wurtzite, silicon

The physical properties of a semiconductor depend on the crystal structure. For instance, the bandgap energy and the effective electron mass are higher in wurtzite (WZ) than in zincblende (ZB) compound semiconductors based on indium.[1] Junctions between different crystal structures in nanowires are atomically sharp and allow for changes in the band structure without modification of the chemical composition.[1,2] In this way, crystal phase quantum dots can be created with extremely high accuracy.[3] The optical properties can also be tuned by a (periodic) stacking of planar defects.[4] Direct optical transitions have been predicted for normally indirect materials such as Ge and Si twinning superlattices (TSL).[5] Consequently, defect and crystal structure engineering are promising routes to tailor properties of nanomaterials.[6]

TSLs have been fabricated in binary semiconductor nanowires[7−11] with the ZB crystal structure via a self-assembly process. However, a TSL in Si with long-range (>20 nm) order has not been reported.[12] Still, a TSL in Si is of particular interest for modifying optical[5] and thermoelectric[13] properties.

Bulk Si has the diamond structure. WZ Si has been fabricated as nanocrystalline domains in matrices exerting a high pressure[14] and appears in nanowires grown by the vapor−liquid−solid (VLS) growth mechanism in the presence of stacking faults.[15−17] Pure, and thus single phase, WZ Si crystals have not been reported so far. Control of the crystal structure in III−V wires has recently been obtained by the use of dopants, V/III ratio and temperature.[7,8,18]

We here report a method to fabricate arrays of pure WZ or diamond TSL Si nanotubes. The desired crystal and defect structure is designed and fabricated in a GaP nanowire and then epitaxially transferred to a Si shell. GaP has been chosen as the template material, because of the relatively small lattice mismatch with Si.

The fabrication of our Si nanotubes requires three main steps: GaP nanowire growth, Si shell growth, and GaP etch (see Figure 1A). The GaP nanowires have been grown via the standard VLS growth method using gold as a catalyst. Substrate conformal imprint lithography was used to fabricate a hexagonal array of Au dots on a GaP (111)B substrate.[19] GaP superlattice

Received: January 19, 2011
Revised: March 3, 2011
Published: March 21, 2011

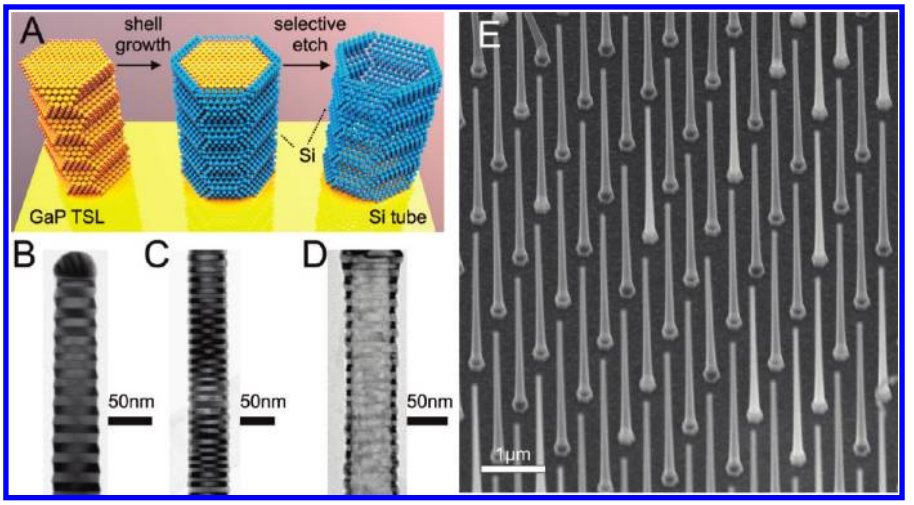

Figure 1. Key steps for the fabrication of a TSL Si nanotubes array. (A) Schematic representation of the fabrication process, accompanied by matching TEM images: (B) a TSL GaP nanowire, (C) a similar nanowire after growth of a Si shell, and (D) remaining Si shell after a selective wet chemical etch step using aqua regia (HNO_3/HCl/H_2O) at 80 °C for GaP and Au. For clarity, the gold catalyst has been omitted in the drawing (A). (E) An overview SEM image of the nanotubes array after completion of the different fabrication steps.

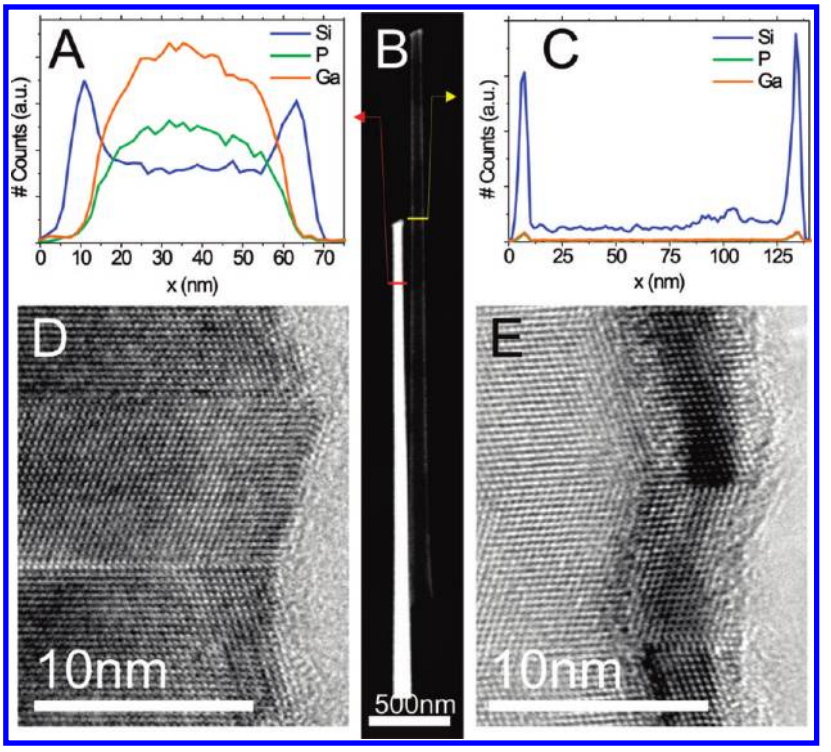

Figure 2. Chemical composition and crystalline quality of GaP/Si core/shell nanowires and Si nanotubes. (A) EDX compositional profile across a GaP/Si core/shell nanowire and (C) across a Si nanotube. (B) HAADF TEM image revealing a completely filled nanowire with a GaP core and Si shell (white) and a Si nanotube (dark). (D) HRTEM image of a GaP/Si nanowire and (E) of a Si nanotube after removing the GaP core.

nanowires were grown in a metal−organic vapor phase epitaxy (MOVPE) reactor using trimethylgallium (TMGa) and phosphine (PH_3) as precursors by adding diethylzinc to the gas phase during growth.[20] In the transmission electron microscopy (TEM) images, shown in Figure 1B, the nanowire features alternating dark and light segments, characteristic for a ZB nanowire with twin boundaries, that is, rotations of the crystal structure by 180° around the long wire axis. The TSL GaP nanowires have the typical {111} side facets with an angle of 19.5° with the growth direction. In the next step, a Si shell has been grown around the GaP template wires at 550 °C using Si_2H_6 as a precursor with a partial pressure of 3.4×10^{-3} mbar, as shown in Figure 1C. The growth parameters for Si have been chosen such that VLS growth is suppressed within the presented growth time range, whereas diffusion-mediated surface growth is facilitated, resulting in a Si shell with a thickness of a few nm (see Supporting Information S1). The alternating dark/light pattern continues across the complete diameter of the wire showing that the TSL structure is transferred

dx.doi.org/10.1021/nl200208q |*Nano Lett.* 2011, 11, 1690–1694

from the GaP core into the Si shell. In analogy to the approach for making semiconductor tubes from core/shell wires,[21−24] the GaP−Si core−shell nanowires were etched in a hot (80 °C) aqua regia ($HCl/HNO_3/H_2O$) solution. First, the Au particle is removed by the etchant solution, and then the GaP core is selectively etched with respect to the Si shell. As a result, Si nanotubes are left behind, as shown in Figure 1D. Furthermore, Figure 1E gives an overview scanning electron microscopy (SEM) image of an array of nanowires, which has been exposed to the etchant solution. Most of the wires (∼90%) are hollow after etching, which becomes clear from the Si nanotubes that appear as dark structures in the array. The cores of the other wires are not etched (bright wires), because a short (4 nm) axial Si segment is formed directly underneath the Au particle. This segment blocks the etchant and as a result the GaP wire remains unaffected.

The GaP/Si epitaxy and the Si shell structure are investigated in more detail in Figure 2. An etched (right, dark) and unetched (left, bright) wire from the same batch are easily recognized by the contrast in the high-angle annular dark-field (HAADF) image in Figure 2B. The etched structures are completely hollow along the whole length of the structure. Energy dispersive X-ray (EDX) line scans across a GaP/Si core shell wire and a hollow Si tube are shown in Figure 2A,C, respectively. The scan in Figure 2A clearly shows a Si shell around the GaP core, and the EDX graph in Figure 2C demonstrates that after etching only the Si part remains and thus a hollow Si tube is created. The Ga and P concentration in the Si tube are below the EDX detection limit (0.3 atomic percent). The Si shell thickness is 8 nm before and 5 nm after etching, which indicates that the Si is also etched by the solution, but at a much lower rate than the GaP. The high-resolution TEM (HRTEM) image in Figure 2D reveals the atomic structure of the GaP/Si core/shell wire. The TSL structure is clearly transferred from the GaP core into the Si shell. Besides the regularly spaced twin planes, no other planar defects were observed in the shells. After etching, the TSL structure is still present as confirmed by the HRTEM image in Figure 2E.

The cross sectional shape of the tubes is revealed by SEM and TEM studies. Because of the small volume, the tubes are semitransparent for electrons and a uniform hexagonal shape is clear from the SEM images (see Supporting Information Figure S1A,B). The exact shape has been determined with TEM and it was found that the average cross sectional shape of the micrometer long Si tube is a hexagon (see Supporting Information Figure S1C). The thickness of the Si shell is the same for the different facets, showing that the growth rate of the Si layer is independent of the polarity of the {111} GaP facets. The thickness of the Si nanotube wall was controlled by the Si growth time (see Supporting Information Figure S2A). Growth times ranging from 2 to 20 min yielded to Si nanotube wall thicknesses ranging from (2 ± 0) nm to (11 ± 2) nm. After 20 min of Si shell growth, Si starts to grow axially by the VLS mechanism (see Supporting Information S1). This axial Si segment prevents etching of the GaP core if it fully covers the section of the nanowire. Because of the very limited thickness of the shells, these tubes are very flexible. Despite their crystalline nature, they can easily be folded (Supporting Information Figure S2B,C). TEM inspection of bent tubes did not reveal any defects, that is, no plastic deformation due to bending was observed.

To tune wire properties, it is important to have control over the segment length. The segment length can be controlled via the GaP TSL nanowire, providing different Ga precursor pressures

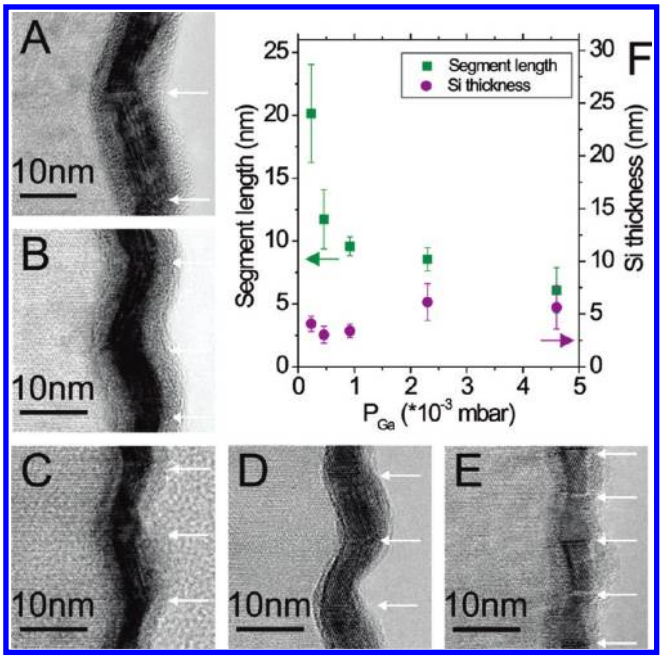

Figure 3. Tuning of the TSL segment length and transfer to Si nanotubes. (A−E) HRTEM images of Si nanotubes. The tubes obtained from GaP core wires grown at different trimethylgallium (TMGa) precursor pressures (2.3×10^{-4}, 4.6×10^{-4}, 9.2×10^{-4}, 2.3×10^{-3}, and 4.6×10^{-3} mbar) resulting in different TSL segment lengths. The GaP core was etched away after Si shell growth. The white arrows indicate the positions of the twin planes. (F) Segment length and Si layer thickness as a function of the Ga partial pressure. The segment length decreases exponentially with the increase in the Ga partial pressure, whereas the Si shell thickness stays constant, as the shell has been grown for a constant Si growth time of 5 min.

during growth. The variation of the segment length with the Ga partial pressure is explained in detail in ref 20. Since the GaP TSL structure is used as a template for the growth of Si, the desired segments lengths are directly transferred to the Si shell. Figure 3A−E are high-resolution TEM images, all taken at the same magnification, of Si nanotubes with different TSL segment lengths. The white arrows indicate the positions of the twin planes. The segment lengths have been plotted versus Ga pressure in Figure 3F. Clearly the Si segment length decreases from (20 ± 4) to (6 ± 2) nm with the Ga pressure (during GaP growth) increasing from 2.3×10^{-4} to 4.6×10^{-3} mbar.

By analogy to the TSL Si nanotubes, the transfer of the WZ crystal structure from GaP to Si is demonstrated next. We note, however, that defect-free WZ GaP has not been reported yet.[25] Therefore, a route was developed for the fabrication of WZ GaP nanowires. HRTEM studies show that GaP wires grown at high temperatures (T = 630 °C) have the WZ structure and they grow along the ⟨0001⟩ direction. The wires have a very low density of stacking faults (few per micrometer), which are perpendicular to the growth direction (see Supporting Information S3). Because of the high temperature, the base (∼1 μm length) of the wires is tapered[26] but the top part has straight facets. GaP−Si WZ nanowires were subsequently fabricated. Interestingly, the growth rate of the WZ Si shells is lower than that of diamond structure shells under identical growth conditions (see Supporting Information Figure S2A). The enhanced growth of the twinned diamond structure is likely explained by the twin plane reentrant edge (TPRE) mechanism. New growth layers are

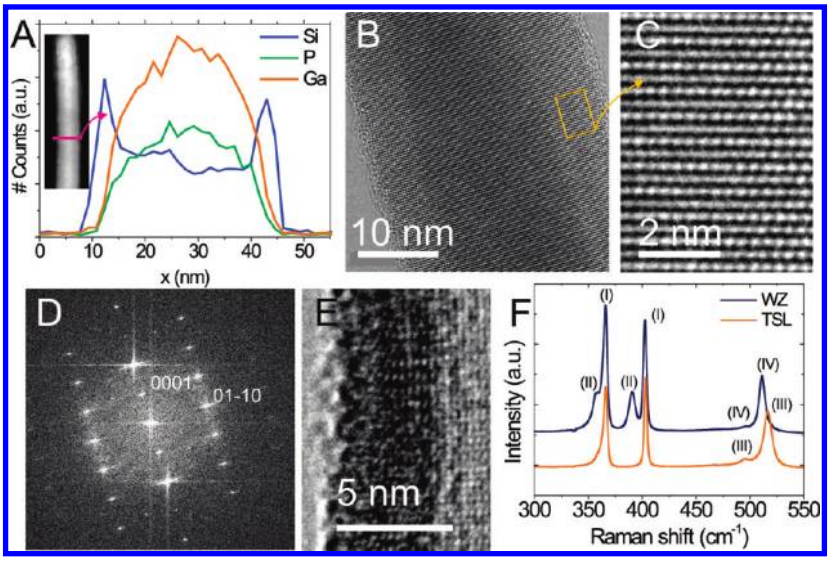

Figure 4. Pure wurtzite GaP/Si core/shell nanowire. (A) EDX compositional profile of a stacking fault-free WZ GaP/Si core/shell nanowire. The inset displays a dark field TEM image of the nanowire. The high-resolution TEM image acquired along the [2-1-10] zone axis displaying (B) the entire diameter and (C) a detail displays the perfect WZ lattice as well as the materials contrast between GaP and Si. (D) The power spectrum (FFT) displays the [2-1-10] zone axis pattern. (E) HRTEM image of a WZ Si tube imaged along the [2-1-10] zone axis. (F) Typical Raman spectra of TSL Si nanotubes (orange solid line) and WZ GaP/Si core/shell nanowires (blue solid line). The roman numerals correspond to characteristic peaks: (I) GaP substrate (366 and 403 cm^{-1}), (II) WZ GaP nanowire (357 and 391 cm^{-1}), (III) TSL Si nanotube (516.5 and 495.6 cm^{-1}), and (IV) WZ Si shell (511.3 and 495.6 cm^{-1}).

preferentially nucleated at a reentrant corner on the nanowire side facets, which corresponds to a twin plane outcrop.[27−29]

The GaP/Si core/shell structure is clearly visible in the dark-field image (see inset Figure 4A). The GaP−Si composition is substantiated by the EDX line scan, displaying the typical shape of a core/shell nanowire (Figure 4A). HRTEM images reveal the WZ Si crystal structure along two independent zone axes [2-1-10] (Figure 4B) and [01-10] (Supporting Information Figure S4), proving the fabrication of a stacking fault-free WZ Si crystal lattice (Figure 4C). Figure 4D displays the fast Fourier transform (FFT) pattern of Figure 4B. The lattice parameters of the hexagonal cell are a = (3.87 ± 0.07) Å and c = (6.61 ± 0.07) Å. The streaking of the spots in the direction perpendicular to the c-axis indicates that the Si lattice of the shell is able to relax in the lateral direction. For all WZ GaP (see Supporting Information Figure S3) and GaP/Si core/shell nanowires structures, a c/a ratio of 1.68 ± 0.01 was found, which is slightly larger than the ideal ratio of 1.63 for close packed hexagonal structures, as also found by Jennings et al.[14,29] Figure 4E shows the wurtzite Si lattice after etching the GaP core. FFT analysis of the HRTEM image yielded a c/a ratio of 1.65 ± 0.02. The larger inaccuracy in this value is due to the flexibility of the Si shell; most of the tubes were slightly bent, leading to broadening of the spots in the FFT patterns. Still, we can conclude that the Si lattice partially relaxes after removal of the GaP core.

Raman spectroscopy studies were performed to substantiate the presence of WZ GaP and Si (Figure 4F) in the backscattering configuration on as grown samples. The 514.5 nm line of an Ar^{+} laser was focused diffraction limited allowing to probe only a few standing nanowires or nanotubes (for further details see Supporting Information S5). The thickness of the WZ and TSL Si shells are both about 4 nm. The transversal optical/longitudinal optical (TO/LO) mode of diamond Si TSL nanotubes, centered at 516.5 cm^{-1}, is downshifted by 4 cm^{-1} with respect to bulk Si, mainly due to phonon confinement,[30,31] which is confirmed by the peak at 495.6 cm^{-1}.

With respect to ZB GaP, the WZ GaP crystal structure gives two additional modes, appearing at 357 and 391 cm^{-1} (indicated by II), as expected from the back folding of the phonon dispersion due to the increased unit cell length.[32] The Si TO/LO mode of WZ GaP/Si nanowires is centered at about 511.3 cm^{-1}. This additional downshift with respect to the TSL Si nanotubes cannot be attributed to confinement effects, since the WZ and the TSL have the same shell thickness. The different peak frequency is thus due to the WZ structure, confirming the TEM results. Strain, due to the presence of the GaP core, has a limited effect on the peak position (see Supporting Information Figure S5).

In conclusion, arrays of standing Si nanotubes with designed crystal structure have been fabricated. Our approach to transfer the crystal and defect structure from one material into another one can be applied to many different material combinations and is therefore a universal tool to control the structural properties of semiconducting materials. This novel way of band gap engineering will allow for new classes of devices combining different crystal structures. Thermoelectric properties of the TSL Si nanotubes are currently being investigated to compare with recent theoretical works on this topic.[33]

■ ASSOCIATED CONTENT

Supporting Information. Additional information and figures. This material is available free of charge via the Internet at http://pubs.acs.org.

■ AUTHOR INFORMATION

Corresponding Author
*E-mail: e.p.a.m.bakkers@tue.nl.

Author Contributions

[#]These authors contributed equally to this work.

■ ACKNOWLEDGMENT

This research was carried out under Project Number MC3.05243 in the framework of the strategic research program of the Materials innovation institute (M2i) (www.M2i.nl), the ministry of economic affairs in The Netherlands (NanoNed). M.H. acknowledges support of the European Community under a Marie Curie IEF Action.

■ REFERENCES

(1) De, A.; Pryor, C. E. Predicted band structures of III-V semiconductors in wurtzite phase. *Phys. Rev. B* **2010**, *81*, No. 155210.

(2) Mattila, M.; Hakkarainen, T.; Mulot, M.; Lipsanen, H. Crystal-structure-dependent photoluminescence from InP nanowires. *Nanotechnology* **2006**, *17*, 1580–1583.

(3) Akopian, N.; Patriarche, G.; Liu, L.; Harmand, J.-C.; Zwiller, V. Crystal Phase Quantum Dots. *Nano Lett.* **2010**, *10*, 1198–1201.

(4) Spirkoska, D.; Arbiol, J.; et al. Structural and optical properties of high quality zinc-blende/wurtzite GaAs nanowire heterostructures. *Phys. Rev. B* **2009**, *80*, No. 245325.

(5) Ikonic, Z.; Srivastava, G. P.; Inkson, J. C. Optical properties of twinning superlattices in diamond-type and zinc-blende type semiconductors. *Phys. Rev. B* **1995**, *52*, 14078–14085.

(6) Perfectly imperfect. (Editorial) *Nat. Nanotechnology* **2010**, *5*, 311−311.

(7) Algra, R. E.; Verheijen, M. A.; Borgström, M. T.; Feiner, L. F.; Immink, W. G. G.; van Enckevort, W. J. P.; Vlieg, E.; Bakkers, E. P. A. M. Twinning superlattices in indium phosphide Nanowires. *Nature* **2008**, *456*, 369–372.

(8) Caroff, P.; Dick, K. A.; Johansson, J.; Messing, M. E.; Deppert, K.; Samuelson, L. Controlled polytypic and twin plane superlattices in III-V nanowires. *Nat. Nanotechnol.* **2009**, *4*, 50–55.

(9) Hao, Y.; Meng, G.; Wang, Z. L.; Ye, C.; Zhang, L. Periodically Twinned Nanowires and Polytypic Nanobelts of ZnS: The Role of Mass Diffusion in Vapor−Liquid−Solid Growth. *Nano Lett.* **2006**, *6*, 1650–1655.

(10) Li, Q.; Gong, X.; Wang, C.; Wang, J.; Ip, K.; Hark, S. Size-dependent periodically twinned ZnSe nanowires. *Adv. Mater.* **2004**, *16*, 1436–1440.

(11) Qin, A. M.; Zhou, X. S.; Qiu, Y. F.; Fang, Y. P.; Su, C. Y.; Yang, S. H. Periodically Twinned Nanotowers and Nanodendrites of Mercury Selenide Synthesized via a Solution−Liquid−Solid Route. *Adv. Mater.* **2008**, *20*, 768–773.

(12) Fissel, A.; Bugiel, E.; Wang, C. R.; Osten, H. J. Formation of twinning-superlattice regions by artificial stacking of Si layers. *J. Cryst. Growth* **2006**, *290*, 392–397.

(13) Hochbaum, A. I.; Chen, R.; et al. Enhanced thermoelectric performance of rough silicon nanowires. *Nature* **2008**, *451*, 163–167.

(14) Jennings, H. M.; Richman, M. H. A Hexagonal (Wurtzite) Form of Silicon. *Science* **1976**, *193*, 1242–1243.

(15) Fontcuberta i Morral, A .; Arbiol, J.; Prades, J. D.; Cirera, A.; Morante, J. R. Synthesis of silicon nanowires with wurtzite crystalline structure by standard Chemical Vapour Deposition. *Adv. Mater.* **2007**, *19*, 1347–1351.

(16) Lopez, F. J.; Hemesath, E. R.; Lauhon, L. J. Ordered Stacking Fault Arrays in Silicon Nanowires. *Nano Lett.* **2009**, *9*, 2774–2779.

(17) Cayron, C.; Den Hertog, M.; Latu-Romain, L.; Mouchet, C.; Secouard, C.; Rouviere, J-L; Rouviere, E.; Simonato, J.-P. Odd electron diffraction patterns in silicon nanowires and silicon thin films explained by microtwins and nanotwins. *J. Appl. Crystallogr.* **2009**, *42*, 242–252.

(18) Joyce, H. J.; Wong-Leung, J.; Gao, Q.; Tan, H. H.; Jagadish, C. Phase Perfection in Zinc Blende and Wurtzite III−V Nanowires Using Basic Growth Parameters. *Nano Lett.* **2010**, *10*, 908–915.

(19) Pierret, A.; Hocevar, M.; Diedenhofen, S. L.; Algra, R. E.; Vlieg, E.; Timmering, E. C.; Verschuuren, M. A.; Immink, W. G. G.; Verheijen, M. A.; Bakkers, E. P. A. M. Generic nano-imprint process for fabrication of nanowire arrays. *Nanotechnology* **2010**, *21*, No. 065305.

(20) Algra, R.E.; Verheijen, M.A.; Feiner, L.F.; Immink, W.G.G.; van Enckevort, W. J. P.; Vlieg, E.; Bakkers, E. P. A. M. The Role of the Surface Energies and Chemical Potential during Nanowire Growth. *Nano Lett.* **2011**, *11* (3), 1259–1264.

(21) Goldberger, J.; He, R. R.; Zhang, Y.; Lee, S.; Yan, H.; Choi, H. J.; Yang., P. Single-crystal gallium nitride nanotubes. *Nature* **2003**, *422*, 599–602.

(22) Hu, J J.; Bando, Y.; Liu, Z.; Zhan, J.; Golberg, D. Synthesis of Silicon Crystalline Tubular Structures with ZnS Nanowires as Templates. *Angew. Chem.* **2003**, *116*, 65.

(23) Noborisaka, J.; Motohisa, J.; Hara, S.; Fukui, T. Fabrication and characterization of freestanding GaAs/AlGaAs core-shell nanowires and AlGaAs nanotubes by using selective-area metalorganic vapor phase epitaxy. *Appl. Phys. Lett.* **2005**, *87*, No. 093109.

(24) Quitoriano, N. J.; Belov, M.; et al. Single-Crystal, Si Nanotubes, and Their Mechanical Resonant Properties. *Nano Lett.* **2009**, *9*, 1511–1516.

(25) Verheijen, M. A.; Algra, R. E.; Borgström, M. T.; Immink, W. G. G.; Sourty, E.; van Enckevort, W. J. P.; Vlieg, E.; Bakkers, E. P. A. M. Three-Dimensional Morphology of GaP−GaAs Nanowires Revealed by Transmission Electron Microscopy Tomography. *Nano Lett.* **2007**, *7*, 3051–3055.

(26) Verheijen, M. A.; Immink, G.; de Smet, T.; Borgström, M. T.; Bakkers, E. P. A. M. Growth Kinetics of Heterostructured GaP−GaAs nanowires. *J. Am. Chem. Soc.* **2006**, *128*, 1353.

(27) Wagner, R. S. On the growth of germanium dendrites. *Acta Metall.* **1960**, *8*, 57–60.

(28) van Enckevort, W. J. P.; Graef, M. W. M. Growth mechanisms of silicon crystallites grown on top of a metal-coated graphite substrate. *J. Electrochem. Soc.* **1981**, *128*, 154.

(29) Note that although the absolute dimensions of the GaP unit cell could not be determined within an accuracy of 0.07 Å in this structure, the c/a ratio is independent of the exact calibration of the image.

(30) Schorer, R.; Abstreiter, G.; Kibbel, H.; Presting, H. Resonant-Raman-scattering study on short-period Si/Ge superlattices. *Phys. Rev. B* **1994**, *50*, 18211.

(31) Schorer, R.; Abstreiter, G.; de Gironcoli, S.; Molinari, E.; Kibbel, H.; Presting, H. In-plane Raman scattering of (001)-Si/Ge superlattices: Theory and experiment. *Phys. Rev. B* **1994**, *49*, 5406.

(32) Zardo, I.; Conesa-Boj, S.; Peiro, F.; Morante, J. R.; Arbiol, J.; Uccelli, E.; Abstreiter, G.; Fontcuberta i Morral, A. Raman spectroscopy of wurtzite and zinc-blende GaAs nanowires: polarization dependence, selection rules, and strain effects. *Phys. Rev. B* **2009**, *80*, No. 245324.

(33) Chen, J.; Zhang, G.; Li, B. Remarkable Reduction of Thermal Conductivity in Silicon Nanotubes. *Nano Lett* **2010**, *10*, 3978–3983.